

Satellite Backscatter Connectivity using Synthetic Aperture Radar

Geneva Ecola[†], Bill Yen[†], Ana Banzer Morgado[†], Bodhi Priyantha[‡], Ranveer Chandra[‡], Zerina Kapetanovic[†]

[†]Department of Electrical Engineering, Stanford University, Stanford, CA

[‡]Microsoft Research, Redmond, WA

ABSTRACT

SARComm is a novel wireless communication system that enables passive satellite backscatter connectivity using existing spaceborne synthetic aperture radar (SAR) signals. We demonstrate that SAR signals from the European Space Agency’s Sentinel-1 satellite, used to image Earth’s terrain, can be leveraged to enable low-power ground-to-satellite communication. This paper presents the first cooperative, on-the-ground target that modulates SAR backscatter to send information bits and analyzes how to extract them from publicly available Sentinel-1 datasets. To demonstrate the system, we evaluate the effectiveness of modulating the radar cross section of corner reflectors both mechanically and electronically to encode data bits, develop a deployment algorithm to optimize corner reflector placement, and present a SAR processing pipeline to enable communication.

1 INTRODUCTION

Despite technological advancements in today’s wireless connectivity solutions, enabling Internet connectivity everywhere on Earth remains an unsolved problem. A vast portion of the planet remains out of reach for smart systems due to a lack of communication infrastructure. Many of the environments most critically impacted by climate change (i.e., oceans and rainforests) are located in remote areas that are inaccessible to existing sensing technologies, and nearly 37% of the population lacks Internet connectivity due to limited resources and government censorship [31]. A connectivity solution that is accessible globally and does not require additional infrastructure could provide vital environmental data and enable a more connected world.

Launching new satellite constellations has taken an important step towards solving this problem by providing broadband connectivity, monitoring the Earth’s ecosystems with remote sensing techniques, and most recently, enabling long-range wireless communication for Internet of Things (IoT) applications [42, 5, 43, 32]. Yet, deploying long-lived sensing systems in remote and resource-constrained environments remains a challenge. Connectivity solutions in remote areas

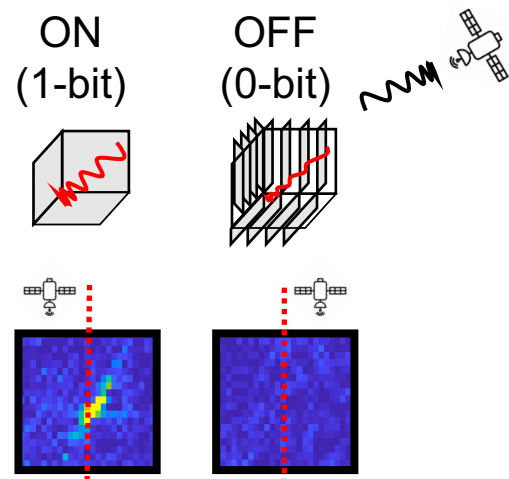


Figure 1: Modulating Synthetic Aperture Radar. The corner reflector modulates incoming SAR signals and separates subsets of data to generate multiple looks of the scene.

must be low-power, cost-effective, and require minimal maintenance. These existing solutions are prohibitively expensive both in terms of launching new satellites to expand their reach and the cost of the service itself [43]. Moreover, new satellites exacerbate issues related to spectrum efficiency, co-existence between space and terrestrial communication networks, and space debris [33, 2]. To this end, we pose the following question: **can we repurpose existing satellite infrastructure to support new low-power methods of ground-to-satellite communication?**

This paper presents SARComm, a new method of enabling passive satellite backscatter connectivity by leveraging existing satellite infrastructure. Our key insight is that instead of relying on active radios and new satellite constellations in an already crowded spectrum, we can exploit signals from satellites already in orbit to enable low-power passive ground-to-satellite connectivity. Our approach leverages satellites equipped with radar systems used for remote sensing applications. Sentinel-1, for example, uses synthetic aperture radar (SAR), which transmits a signal and observes the received backscatter to gain insights into Earth’s terrain and generate

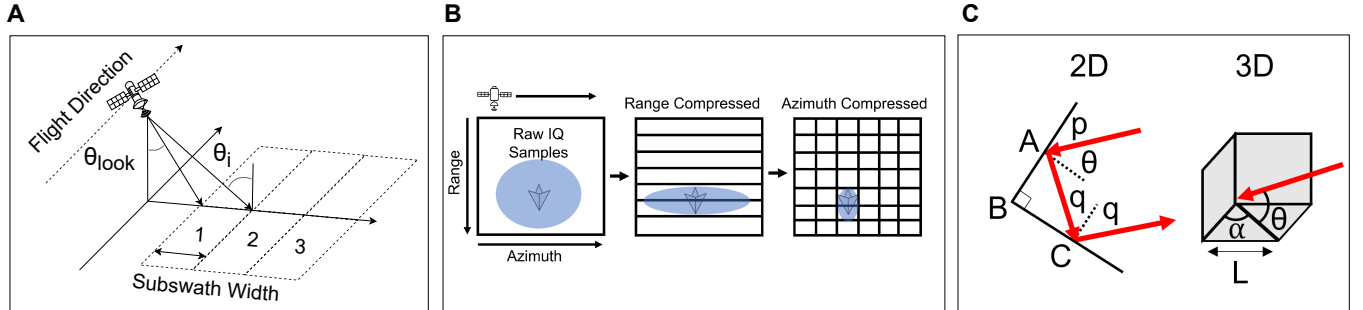


Figure 2: Background on SAR and Corner Reflectors. (A) shows the three subswaths from the IW mode of the satellite and the incidence angle (θ_i) and look angle (θ_{look}) as defined by Sentinel-1. (B) depicts an overview of SAR data processing. (C) is an illustration of a square trihedral corner reflector where the reflected ray is parallel with the incident ray for a range of values of θ . The RCS of the corner reflector is dependent on the side length (L) of the square panel, and maximum RCS is achieved when the incidence angle is parallel to its bore-sight direction.

images [44]. Sentinel-1 is designed to receive backscatter signals and, therefore, presents an opportunity to reuse its ambient satellite signals to enable long-range and low-power backscatter communication. Similar to RFID, a satellite imaging system could act as the reader for low-power devices on the ground that modulate existing signals. By changing the reflectivity of an object on the ground, it is possible to modulate the spaceborne SAR signals and wirelessly transmit information bits with near zero power.

However, compared to existing ambient backscatter techniques, this is quite challenging. Sentinel-1 has an imaging resolution of 22x3 meters and is hundreds of kilometers away from Earth [4], meaning that the target on the ground needs to have a very large radar cross section (RCS) in order to detect any change and have a stronger backscattered signal than the surrounding environment. Moreover, Sentinel-1 typically collects data every 12 days (some areas are imaged more frequently), and for any particular area of interest, the data collection period is on the order of hundreds of milliseconds [36]. Lastly, while Sentinel-1 data is publicly accessible, existing data processing techniques are designed for imaging and not communication, thus requiring the development of a new data processing pipeline. Finally, the data must be retrieved and processed without introducing custom satellite hardware or new terrestrial infrastructure (e.g., ground stations) to make it accessible for all.

SARComm solves these challenges by leveraging corner reflectors as cooperative on-ground targets to maximize RCS and designing them to switch between reflective and non-reflective states, as illustrated in Figure 1. This allows SARComm to wirelessly transmit information by modulating an incoming SAR signal. To ensure that data can be reliably transmitted, we develop a deployment algorithm to optimize the RCS of a corner reflector by identifying locations with

minimal background clutter for any given region and determining the optimal angle and orientation during the satellite pass. To increase data rate beyond what existing Sentinel-1 SAR data processing techniques allow (a single resolved image per pass), SARComm uses a new data processing pipeline that enables multiple bits of data to be extracted by producing multiple images each time the satellite passes. **We make the following key contributions:**

- (1) We present a new method to enable passive satellite backscatter connectivity using the Sentinel-1 Mission.
- (2) We develop an algorithm that identifies optimal corner reflector deployment sites within a region of interest and provides the ideal reflector tilt angle and bearing.
- (3) We design modulated corner reflectors to manipulate the reflectivity of objects on the ground and observe these changes at distances as far as 693 km [44] using spaceborne synthetic aperture radar.
- (4) We introduce a new SAR processing pipeline for wireless communication and extract changes in target reflectivity during a single satellite pass.

2 BACKGROUND

Synthetic Aperture Radar (SAR) is a type of active remote sensing that involves transmitting RF signals and observing the backscattered signal to infer the physical characteristics of ground targets [44]. It has many applications, such as glacier monitoring and forest biomass estimation [44]. Often, corner reflector calibration targets are used for SAR systems; corner reflectors are on-ground devices that appear very brightly in SAR images [24]. SARComm leverages both SAR systems, specifically the Sentinel-1 mission, and corner reflectors to enable satellite backscatter connectivity. In this section, we provide a background on Sentinel-1, SAR signal processing, and corner reflector theory.

2.1 Sentinel-1 Mission

The ESA's Sentinel-1A is a low Earth orbit (LEO) satellite deployed 693 km above the Earth's surface and operates in the C-band (5.4 GHz) [6, 8]. The reflections received as the satellite is in motion are stitched together to form a much larger synthetic antenna than the physical antenna on the satellite [45]. SAR systems can image the Earth at all times of day regardless of weather conditions [8]. Data collected by Sentinel-1 comes in 12-day cycles made up of a set of defined relative orbit paths, with some locations revisited more frequently than others [6].

2.1.1 SAR Signal Processing. SAR processing is typically done in two steps: range and azimuth compression [23]. At a high level, the raw IQ data is sorted into range and azimuth bins to form the pixels of the resolved image, as shown in Figure 2B. SAR systems transmit linearly frequency-modulated signals called chirps and receive the backscatter (also referred to as echoes) after it reflects off of Earth's surface. Given the time that it takes these echoes to return and the known shape of the chirp, range compression is performed to sort the echoes into range bins [23]. The chirps are transmitted at a defined pulse repetition frequency (PRF), which is frequent enough such that any area of interest is characterized by multiple receive echoes as the satellite passes overhead [8]. Using the Doppler shift caused by the known movement of the satellite allows it to differentiate return echoes from targets along the azimuth direction in a process called azimuth compression [23].

2.1.2 Acquisition Modes. While Sentinel-1 has several acquisition modes, Interferometric Wide Swath (IW) is primarily used, covering most of the land on Earth. In IW mode, the radar uses beam steering to increase the coverage area and to provide more consistent resolution in the image [4]. The beam is steered to capture separate areas in the azimuth direction called bursts and between three different range sections called subswaths. The subswaths along, with the look angle (θ_{look}) and incidence angle, (θ_i) which define the angle of the SAR signals, are shown in Figure 2A. The main drawback of IW mode is that less time is spent imaging the same location, reducing the final image's azimuth resolution. IW modes achieve a range resolution of about 3 m and azimuth resolution of 22 m [4]. In this mode, two polarizations are measured, co-polarization (VV) and cross-polarization (VH).

2.1.3 Data Format and Accessibility. The data collected by Sentinel-1 is provided at different levels. Level 0 is the measured echo of the radar represented as encoded raw IQ samples. Level 1 data is a resolved image where the raw samples have been compressed in the range and azimuth directions [3]. SARComm uses Level 0 data for processing.

Sentinel-1 data is publicly available and can be accessed through the Alaskan Satellite Facility (ASF) using ASF Vertex [35].

2.2 Corner Reflector Theory

Corner reflectors are retroreflectors that passively redirect RF waves back to their emission source. RCS defines how much an object reflects signals back at the source. The square trihedral corner reflector consisting of three square planes has the largest maximum RCS (σ) among typical reflector designs, where RCS is given by the expression below,

$$\sigma_{max} = \frac{12\pi L^4}{\lambda^2} \quad (1)$$

where L is the side length of the square panel of the reflector as shown in Figure 2C and λ is the wavelength of the incident RF wave [47, 34]. The maximum RCS is achieved when the incidence angle is parallel to boresight, meaning that α is 45° and θ is 35.26° [19] from Figure 2C. The reflector's RCS defines how much signal will be reflected back and is used in the radar equation to calculate the expected receive power (P_r) from a target,

$$P_r = \frac{P_t G^2 \sigma \lambda^2}{(4\pi)^3 r^4} \quad (2)$$

where P_t is the transmit power, G is the antenna's gain, and r is the distance from the target [34]. Signal to Clutter Ratio (SCR) is often used in SAR applications to describe the ratio of a target's power to the backscattered power from the surrounding environment.

3 SARCOMM SYSTEM DESIGN

SARComm implements backscatter communication using Sentinel-1's existing satellite infrastructure to enable a low-cost and low-power connectivity solution for extremely resource-constrained environments. As shown in Figure 3, SARComm has four key components: a reflector deployment algorithm, a modulated corner reflector, a satellite receiver, and a data processing pipeline.

- **Reflector Deployment Algorithm.** The deployment algorithm informs where and how to deploy a reflector by optimizing its RCS as seen by the satellite. It takes into account terrain, satellite orbit information, and historical Sentinel-1 SAR data to specify the optimal location, angle, and size of the corner reflector for deployment.
- **SARComm Modulated Corner Reflector.** The modulated corner reflector is a device that switches between a reflective and non-reflective state using either mechanical or electronic approaches, which transmits data via amplitude-shift keying (ASK) modulation. To maximize

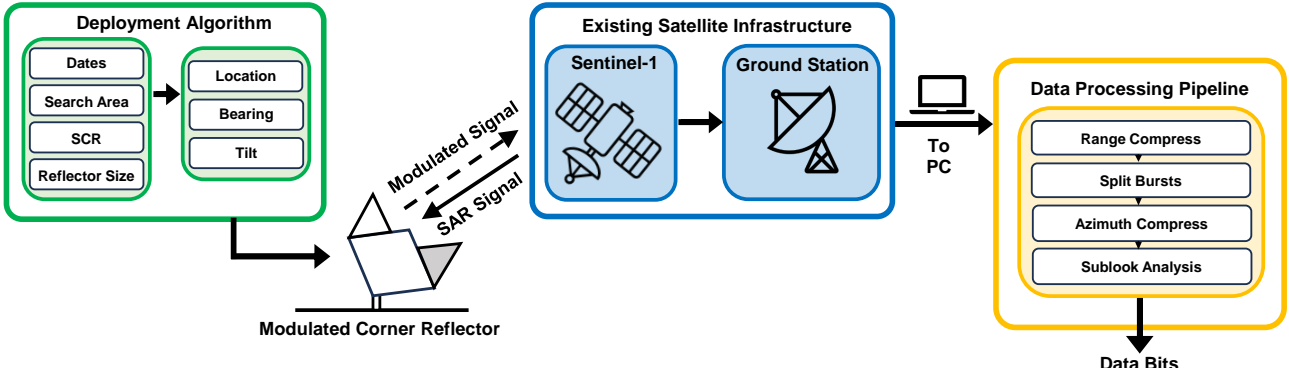


Figure 3: System Design of SARComm. This proposed system enables ultra-low power, long-range communication using the existing Sentinel-1 infrastructure by introducing a cooperative on-ground target in the form of a modulated corner reflector. A placement algorithm determines the optimal location for the reflector, and a standard PC with access to the Internet can run a data processing pipeline to extract the information bits the satellite receives.

the data rate during the brief period of time that the reflector is imaged, the corner reflector must be able to rapidly switch between different states while remaining detectable by the satellite.

- **Sentinel-1 as a Receiver.** SARComm does not require deploying new satellite infrastructure. Instead, it uses the existing Sentinel-1 satellite by modulating its backscattered signals and extracting the information sent by the reflector from ESA's publicly available Level 0 data.
- **Data Processing Pipeline.** Existing SAR data processing techniques are not designed for communication. Therefore, a new process is developed to split SAR datasets from a single satellite pass and produce separate time-independent sublook images such that multiple states of the reflector can be extracted. This data processing pipeline has four major steps: range compression, burst splitting, azimuth compression, and image analysis of each sublook image to determine the state of the reflector.

3.1 Reflector Deployment Algorithm

A key challenge with designing a satellite backscatter system is the significant distance (100s of km) between the satellite receiver and the modulating device on the ground. To implement ASK using the SAR backscatter signals, the device on the ground must be visible. The deployment algorithm addresses how one can optimize the placement and angle of corner reflectors to ensure the best performance of the communication system.

3.1.1 Finding Low Clutter Locations. The algorithm first identifies the optimal deployment site within a user-defined area for each relative orbit of the satellite that images that location. This process commences by pulling historical Range Terrain Corrected (RTC) data from Planetary Computer's Data Catalog [41] over a user-specified date range to analyze

a location's clutter levels. This allows the user to analyze the scene with recent or historical data to deal with issues such as seasonal changes in the site due to rain. This process is illustrated in Figure 4. For context, a satellite camera image of the area used for an example of this analysis is shown in Figure 4A.

To find low clutter areas, all Sentinel-1 datasets that meet the specified input parameters are downloaded and averaged together, shown in Figure 4B. This reveals that the grassy field has much less radar clutter than the man-made objects surrounding it. Next, the averaged image is thresholded to remove high clutter locations. After that, an erosion algorithm is applied to the binary image to find specified areas (kernels) that are not only low clutter in of themselves but are also surrounded by neighbors with low clutter. The results of both threshold and erosion are in Figure 4C, which shows the two binary images summed together. This operation results in an image where white pixels are locations above the threshold value, gray pixels are at locations that were eroded (meaning they were low clutter but too close to high clutter areas), and black pixels at locations that are both low clutter and surrounded by low clutter. In Figure 4D, the largest low clutter area is annotated on the average SAR image to suggest a low clutter deployment area, minimizing interference from background clutter.

3.1.2 Optimal Bearing and Tilt Angle. Once an ideal location is determined by the low clutter algorithm, the optimal bearing, as shown in the top view in Figure 5, and tilt angle, shown in side view in Figure 5, can be selected. The boresight of the reflector must be facing toward the satellite and aligned with the incidence angle of the incoming SAR signals. To determine the bearing, the relative orbit of the satellite is used to calculate the cardinal direction that the reflector should face. The algorithm outputs angles between

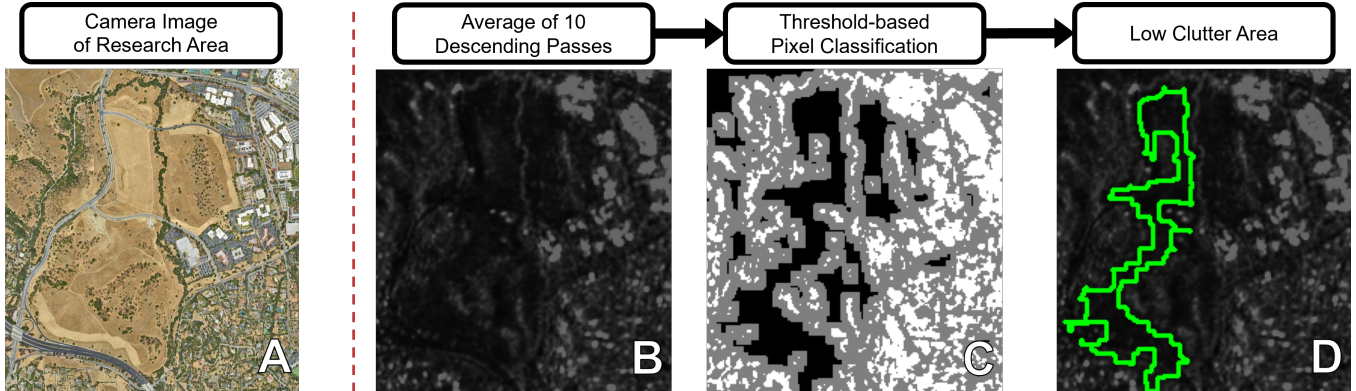


Figure 4: Low Clutter Algorithm Overview. (A) Camera Image of Research Area [30], (B) Average of 10 previous descending passes of this location with lighter colors representing brighter areas, (C) White pixels are above the threshold, gray is below but has bright pixels near it, and black pixels are low clutter pixels surrounded by low clutter pixels, and (D) Average SAR Image annotated with low clutter area (green).

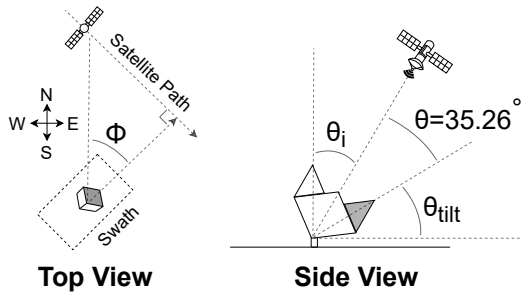


Figure 5: Optimal Tilting and Bearing Angles of the Reflector. The angle that the bottom panel of the corner reflector (shaded grey) tilts to (θ_{tilt}) should be complementary to the sum of the incidence angle (θ_i) and 35.26° (see Section 2.2). To maximize RCS, the corner of the bottom square panel should point perpendicular to the satellite path in the bearing angle Φ relative to the north.

0° and 359° , with zero degrees being due north. This matches how any compass, such as those available on smartphones, presents angles. Similarly, the range location of the chosen deployment site within the imaging swath is used to determine what the incidence angle of the SAR signals will be and, therefore, how the reflector should be tilted. The tilt is calculated by subtracting the incidence and boresight angles, 35.26° from 90° [19].

3.2 Modulated Corner Reflectors

Enabling satellite backscatter using SAR signals requires modulating a cooperative on-ground target (in this case, a corner reflector) such that it can switch between reflective and non-reflective states. Achieving this requires addressing several design requirements:

- **Radar Cross Section.** The reflector must have a large enough RCS to be detectable from the background clutter

within the radar image, as the expected receive power at Sentinel-1 is directly related to RCS (see Equation 2). The specific required RCS depends on many of the factors described in Section 3.1, as well as the type of processing done, but in general the length of a corner reflector, L as shown in Figure 2C, should be at least 10x the wavelength of the signal [37]. In the case of Sentinel-1, this means a reflector's side length should be at least 0.56 m, equating to an RCS of 1202.9 m^2 , which is known to show up well in Sentinel-1 datasets even in high clutter areas [28].

- **Signal to Noise Ratio.** The reflector must create a large enough contrast between its ON (reflective) and OFF (non-reflective) states to distinguish state changes from the noises in the system. In typical ASK modulation, the amplitude of the signal is inversely proportional to the probability of bit error [13]. Therefore, increasing the change in RCS between states would improve the theoretical data rate of the system. Sentinel-1's radiometric resolution ($<1 \text{ dB}$ in IW mode) is the dominant driving factor for the reflector's minimum reflectivity contrast [7]. Further, processing SAR data to produce multiple images over time degrades the signal resolution (see Section 3.4). As such, a minimum state contrast of 10 dB was chosen to distinguish state changes from distortions sufficiently.
- **Data Rate.** Given that Sentinel-1's pass is extremely short, there is a minimum data rate that must be achieved in order to extract information from the backscattered signal. This translates to optimizing the switching speed of the reflector, which first requires understanding the total time Sentinel-1 spends imaging to generate a single pixel. The time spent per pixel (t) can be approximated as l/v , where l is the width that the satellite's beam covers the ground and v is the velocity of the satellite. The velocity is given by $v = \sqrt{G \times M_{central}/R_{Earth} + H} = 7.45 \text{ km/s}$

Table 1: Corner Reflector Design Requirements.

Requirement	Value
Min. RCS (Reflective (ON) State)	1202.9 m ²
Min. State Contrast	10 dB
Max. Switching Duration	108 ms

where $G = 6.673 \times 10^{-11}$, $N \cdot m^2/kg^2$, $M_{central}$ and R_{Earth} being the mass and radius of the Earth respectively, and H being the height of the satellite [17]. On the other hand, l is related to the satellite's beamwidth (w_{beam}) by the expression $\tan(w_{beam}/2) = l/d$ where d (ground distance between the satellite and the target) equals the altitude of the satellite multiplied by the tangent of its look angle. Consider the worst-case scenario where the reflector is located at the nearest edge of the satellite's beam, the look angle will be about 30° , which gives $d=400$ km. This results in $l=1.61$ km using a $w_{beam}=0.23^\circ$ and $t=216$ ms [8]. One particular Sentinel-1 chirp was captured to validate the signal duration, which ended up being 332 ms (see Figure 6). This value is larger than the minimum duration calculated since the illuminated spot is beyond the nearest edge of the satellite's beam. To reliably transmit state changes throughout this period, the switching duration should be at most half the minimum imaging duration for the pixel (108 ms). However, the switching speed should be maximized, as it directly affects the system's data rate. The quantified design requirements for the modulated reflector are summarized in Table 1.

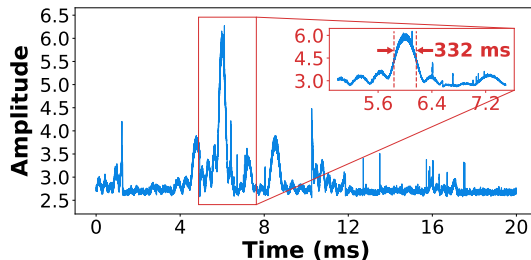


Figure 6: Sentinel-1 Signal. Sentinel-1 radar signals detected using a dish antenna [26] (arbitrary amplitude unit). The signal shows that the radar illuminated the location for 332 ms when thresholded at -3 dB of the peak value.

3.3 Reflector Design

There are two approaches to designing a modulated corner reflector: mechanically or electrically controlled.

3.3.1 Mechanical Modulation. A corner reflector generates an extremely large RCS using three orthogonal panels to bounce signals back to their source. Therefore, changing the

angles of these panels relative to one another has a drastic effect on its RCS [10]. In fact, the contrast between perfectly aligned and misaligned panels is quite large, where deviating panel angle by just 2° can have a transmission loss on the order of 30 dB for large reflectors [10].

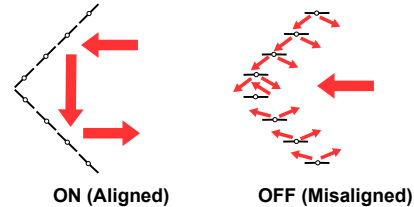


Figure 7: Mechanical Modulation Design. The incoming radar signal scatters when the sub-panels are misaligned, resulting in less signal being returned to the satellite and therefore a smaller RCS.

We have designed a mechanically modulating reflector that exploits this effect to generate a large difference in the RCS of the device, which is realized by splitting each reflector panel into four sub-panels that can be tilted. When the sub-panels lay flush, the reflector behaves as normal. When the panels are rotated, they become misaligned such that the incoming signal is scattered in undesirable directions instead of back to the satellite, thus decreasing the RCS as illustrated in Figure 7. A $2' \times 2'$ panel dimension was chosen to generate a maximum RCS of 1689 m², which meets the minimum RCS specification from Table 1. Depending on the necessary panel displacement, many commercial motors are capable of actuating in the 30-40 ms range, which makes mechanically modulated reflectors a potentially viable option for achieving the necessary switching speed.

3.3.2 Electronic Modulation. Another method of modulating the RCS of a corner reflector is by selectively reflecting or absorbing the incoming RF signal instead of allowing it to scatter. A corner reflector's panels are highly reflective, but by introducing an absorptive element, namely a well-placed antenna, we can reduce the amount of backscattered signal. Prior work has shown that an antenna located half wavelength away from the vertex of the corner reflector will maximize the gain at said frequency [29]. Similar to traditional backscatter systems, when the antenna is impedance matched to its input load, it is expected to absorb most of the signal the antenna receives, and when it is mismatched, the signal will be reflected back to the satellite, thus enabling ASK modulation (see Figure 8). Since typical corner reflector antennas feature two orthogonal reflective panels and a dipole antenna [29], the introduction of a third panel effectively creates a monopole antenna with a highly directional radiation pattern with the three grounded reflector panels.

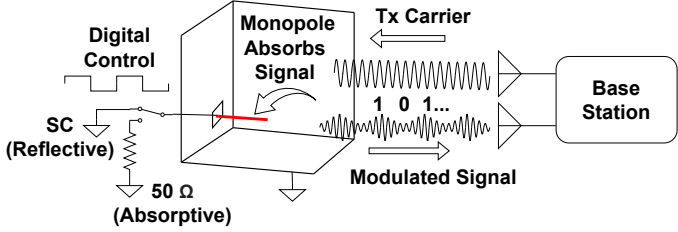


Figure 8: Electrical Modulation Design. A monopole antenna connected to a matched ($50\ \Omega$) and short circuit (SC) load through an RF switch allows the corner reflector to switch between absorptive and reflective states, which enables ASK modulation.

Typical RF switches operating at Sentinel-1's frequency range have switching times in the order of a few nanoseconds and ultra-low power consumption ($< 3\ \mu\text{W}$) [20]. This makes electronically modulated corner reflectors a potentially better solution than mechanically modulated reflectors in terms of data rate and energy efficiency.

3.4 SAR Processing for Communication

The simplest realization of a SAR backscatter communication system would involve using a target with two configurable brightness levels to communicate a single bit every time the satellite images the area (e.g., every 12 days). However, this approach has clear practical limitations. To achieve a higher throughput, SARComm requires SAR processing techniques that can extract several bits of data in a single pass, which is much more challenging compared to the aforementioned strawman approach.

SAR processors are designed to produce one high-resolution image per pass. This is achieved through range and azimuth pulse compression, where many different radar pulses contribute to the value at any one pixel in the image. The name "synthetic aperture" refers to the synthetically large antenna that is generated by the movement of the satellite, which enables SAR to achieve its impressive resolution in the azimuth direction [45]. SARComm takes a different approach, where the aperture is divided to generate multiple lower-resolution images rather than using the full aperture to generate one high-resolution image [40]. In SAR processing, this technique is often called "multi-looking," "sublooking," or "subaperture processing," and it is primarily used to reduce speckle noise in images. We leverage the subaperture processing technique for a novel application: enabling backscatter communication of multiple data bits during a single satellite pass.

Subaperture processing generates uncorrelated sublook images by processing each image using different subsets of the data [40]. When this is done in the azimuth direction, it creates images that capture the scene at different center times [38]. This means that subsets of data will use the echoes

from different points in the satellite's trajectory. The main drawback of this approach is that it worsens the azimuth resolution of the image, which is given by $p_x = D/2$ where D is the length of the system's physical antenna [40]. Subaperture processing will increase this by the number of sublooks (N) to $p_x = ND/2$ assuming the aperture is split into equal-sized pieces. While the range resolution of the image will remain the same. Using this approach, the reflector can be modulated such that the state of the reflector, reflective or non-reflective, can be detected within the subimages. Figure 9 shows a basic overview of how the original SAR processing pipeline (Figure 2B) is adapted to achieve subaperture processing.

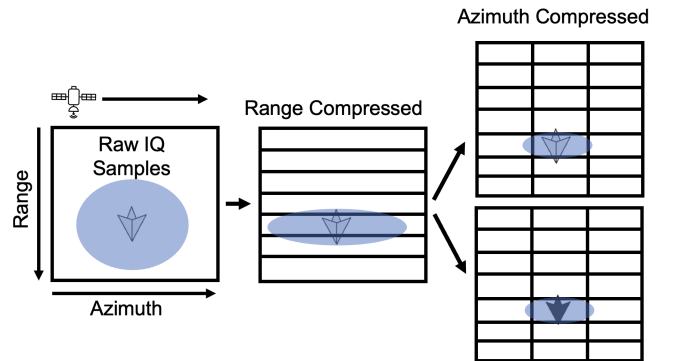


Figure 9: Subaperture Processing to Produce Separate Time-Independent Images. This allows for the extraction of multiple ground target states over the span of a single satellite pass.

3.4.1 Impact of Sublooking. The amount of data that can be sent using this communication system will depend on how many times the aperture can be split while still being able to detect the reflector. This is impacted by several factors including the amount of time over which the area is imaged, the background clutter level, the size of the reflector, and the difference between its ON/OFF states. To analyze the impact of this reduced image quality, a model of the reflector's normalized RCS is shown in Figure 10.

In Figure 10, the normalized RCS is shown for several sizes of corner reflectors. Typical levels of clutter are also shown, and these can vary widely. For instance, there is clutter in large cities that is brighter than a $4' \times 4'$ corner reflector, and there are also areas of extremely low returns on large bodies of water like the ocean. The difference between the corner reflector's normalized RCS and the clutter level in the background will define the SCR of the scene. This shows that while subaperture processing decreases the signal from the corner reflector, the SCR of the sublooks will remain consistent if the background clutter remains constant.

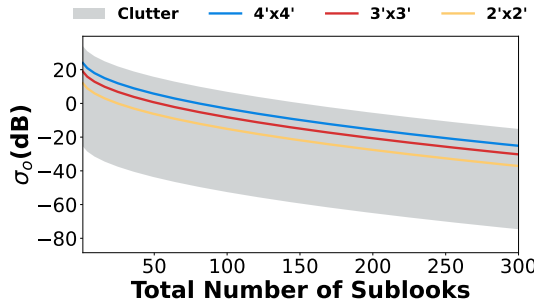


Figure 10: RCS vs. Total Number of Sublooks. The normalized RCS decreases as the number of sublooks increases during subaperture processing.

3.4.2 Properties of Sublook Images. It is important to understand what to expect from each sublook image itself. As mentioned before, each sublook will represent a different center point in time. The difference of center time between sublooks is given by $\Delta t = n_s/PRF$, where n_s is the number of radar echos used for each sublook and PRF is the pulse repetition frequency of the radar. As calculated in the modulation speed requirement above, there will typically only be around 100 to 200 ms available to send data. With a PRF of 1.7 kHz, this means that each azimuth line will have around 200 to 400 data lines. Therefore, at a certain point, the aperture will also be limited by splitting because at least one line is needed for each sublook. Additionally, it is important to understand how the amplitude of the reflector will vary across sublooks. According to [22], the relationship between the RCS of a square corner reflector (σ) and the azimuth (θ) and elevation (ψ) angles is the following:

$$\sigma(\psi, \theta) = \begin{cases} \frac{4\pi}{\lambda^2} L^4 \left(\frac{4c_1 c_2}{c_3}\right)^2 & \text{for } c_2 \leq \frac{c_3}{2} \\ \frac{4\pi}{\lambda^2} L^4 \left(c_1 \left(4 - \frac{c_3}{c_2}\right)\right)^2 & \text{for } c_2 \geq \frac{c_3}{2} \end{cases} \quad (3)$$

where c_1 , c_2 , and c_3 are $\sin\psi$, $\cos\psi/\sin\theta$, and $\cos\psi/\cos\theta$ such that $c_1 \leq c_2 \leq c_3$. L and λ represent the interior length of the reflector panels and the nominal wavelength respectively. Since Sentinel-1 moves only in the azimuth direction, we can assume $\psi=35.26^\circ$ throughout the entire pass. The possible variation in θ will be given simply by half the beamwidth of the antenna, which is 0.115° . Using these angle values and an $L=2'$ at 5.4 GHz, the maximum change in σ from Equation 3 is only about 0.006 dB, meaning that the corner reflector will have approximately the same amplitude in each sublook. This simplifies the analysis of the system considerably, as the SCR ratio should be consistent across sublooks.

4 SARCOMM EVALUATION

To evaluate SARComm, we built and deployed corner reflectors to analyze their SCR for various environments. Through these deployments, we validate the effectiveness of the deployment algorithm. Next, we implement both mechanically

and electronically modulated corner reflectors in the lab to evaluate their performances. The mechanically modulated reflector was then deployed in the field to collect data for the SAR processing pipeline. Finally, we examine the performance of the pipeline to extract bits using data collected from the aforementioned field experiments.

4.1 Deployment Algorithm Results

4.1.1 Implementation. To evaluate the effectiveness of the deployment algorithm, we designed and implemented three square trihedral corner reflectors with panel sizes of 2'x2', 3'x3', and 4'x4' ft and theoretical maximum RCSs of 32.4, 39.3, and 44.4 dB, respectively, at 5.4 GHz (see Figure 11). The reflectors feature three square aluminum panels of their respective sizes and a frame that secures the panels in order to ensure their perpendicularity and elevate the panels from the ground. Among the different designs implemented, we found that 80/20 aluminum extrusions provided the best combination of strength-to-weight ratio and ease of assembly for the reflector frames [1]. The frames are designed such that they can be taken apart and assembled in outdoor deployments. The corner reflectors were deployed at three different geographical locations within the United States: a dry lake bed (desert), a soccer field (grass field), and a natural field surrounded by rolling hills (grassy hill). For each deployment, the GPS coordinates of the reflector location were logged, and level 1 data was downloaded from ASF [35] and analyzed in SNAP [9].

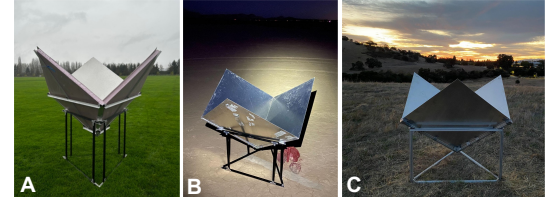


Figure 11: Reflector Deployments. (A) 4'x4' in grassy field, (B) 2'x2' in desert, (C) 3'x3' in grassy hill.

4.1.2 Results. Figure 12A-H show the 2'x2', 3'x3', and 4'x4' corner reflectors across a range of deployment conditions. In Figure 12A and 12E, the same 2'x2' reflector showed up in a clear desert field, but not on the grassy hill. This is likely due to a number of factors, including the difference in background clutter and the unwanted tilt on the hill as opposed to the flat desert floor. Flat areas like water and desert typically have specular reflections that redirect backscatter away from the satellite and thus look less cluttered, as opposed to the more diffuse reflections from rougher surfaces like grassy areas. The effects of weather on SCR can likewise be seen between Figure 12B and 12F, where the surrounding grounds

show up significantly brighter after rain, making the corner reflector less distinguishable from the clutter.

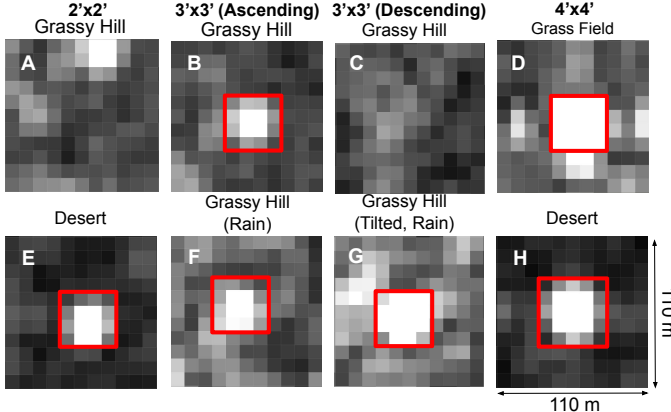


Figure 12: Static Corner Reflector Results. The co-polarization amplitude of the corner reflectors (red) as seen by Sentinel-1 under various deployment conditions.

All of the reflectors except 12G were placed with the boresight direction of the reflector pointing straight up. Given that the incidence angle of Sentinel-1 in IW mode is 30° to 45° (see Figure 5), pointing the boresight straight up will cause a reduction in the measured RCS. The satellite's trajectory relative to the reflector's location also affects how the reflector is imaged since Sentinel-1 always scans to its right. As seen between Figure 12B and 12C, the 3'x3' reflector placed at the same location does not show up on a clear day during a descending pass even though one could clearly identify it during an ascending pass despite rainy conditions the night before. This can be mitigated by angling the reflector toward the direction of the satellite pass and then tilting its boresight to match the incidence angle of the satellite radar as presented in Figure 5.

The average σ_0 , or the radar reflectivity per unit area in the ground range, increased from 0.1366 to 0.4417 between Figure 12F and 12G just by improving the reflector's orientation. Lastly, due to the dependence of RCS on the size of the reflector, larger reflectors tend to have much better RCS (see Figure 12E vs. 12H).

4.2 Mechanically Modulated Reflector

4.2.1 Implementation. To implement the mechanical modulation described in Section 3.3.1, a 2'x2' reflector was constructed where each side of the corner reflector is divided into four panels that are controlled by servos so that they rotate to the same positions synchronously [25]. In order to optimize for state contrast and modulation speed, we conduct a control experiment to measure the received signal strength of the backscattered signal for both ON and OFF

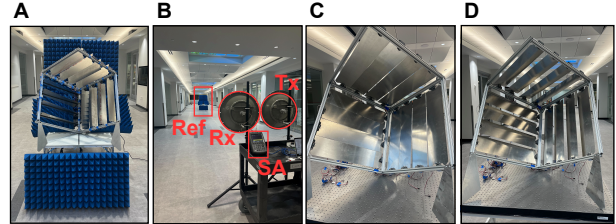


Figure 13: Mechanically Modulated Corner Reflector. (A) shows the corner reflector setup with absorptive foam to reduce background clutter (B) shows the test setup (C) shows the reflector in its ON state and (D) shows the reflector in its OFF state.

states while varying both switching duration and panel angles. Figure 13A-D shows the mechanically modulated corner reflector, the experimental setup, and the reflector in the two switching states. The reflector was placed 19 m away from a transmitter and receiver to ensure it was in the far field, and RF absorber foam was placed around it to reduce clutter (see Figure 13A). A USRP software-defined radio connected to a 30 dBi C-band dish antenna to transmit a continuous 5.75 GHz tone (in the ISM band and near Sentinel-1's operation frequency) at -16.23 dBm, and the backscattered signal was received using a spectrum analyzer connected to an identical antenna [26]. These antennas feature a very narrow beamwidth, which makes crosstalk and interference minimal despite their proximity. The reflector is shown in its ON state in Figure 13C, and OFF state in Figure 13D.

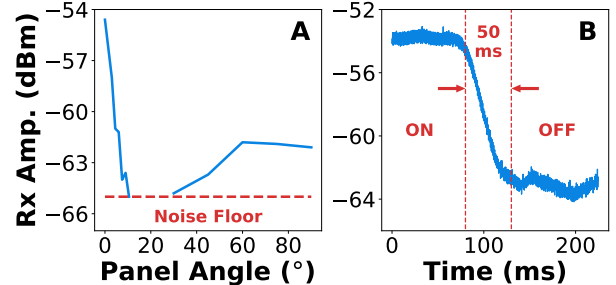


Figure 14: Mechanical Modulation Result. (A) The modulated mechanical reflector's reflected signal disappears below the noise floor after rotating its panels approximately 12° from their flat position. (B) The maximum amplitude change between states is 10.89 dBm, and it takes 50 ms for the reflector panels to rotate the full 12° .

4.2.2 Results. In Figure 14A, the amplitude of Rx power reaches its minimum value (below the noise floor) when the panels are tilted at 12° from their flat positions, creating a >10 dB contrast from their flat state. Due to the speed constraint from these motors, the shortest time during which the panels can achieve this range of motion is about 50 ms,

with shorter toggling periods resulting in dramatically lower amplitude changes since the panels could not make the full 12° turn. As such, the mechanically modulated reflector is marginally able to meet the toggling duration requirements set in Section 3.2 with a limited bit rate. The measured receive power in the ON state is -54.6 dBm, which is slightly higher than our theoretical value of -55.8 dBm from Equation 2. This difference can be attributed to reflections from the background clutter that got picked up by the edge of the antenna beamwidth. Figure 14B demonstrates a 10 dB amplitude change of the Rx waveform from the mechanically modulated reflector when switching every 50 ms at 12° .

4.3 Electronically Modulating Reflector

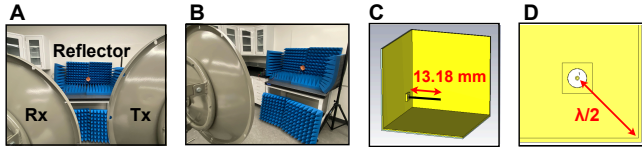


Figure 15: Electronically Modulated Corner Reflector. (A) and (B) show the experimental setup to evaluate the active corner cube. RF absorber foam is placed around the corner cube to minimize background reflections. (C) and (D) show the simulated design of the active corner cube.

4.3.1 Implementation. A bench-scale version of the electronically modulated reflector is constructed out of three pieces of single-sided 70x70 mm FR4 boards with the copper plating facing the inside and soldered together to ground. We integrated a monopole feed into the corner reflector, which absorbs the Tx signal when the feed impedance is matched with its load. The monopole antenna was designed in Ansys HFSS [11] to have a simulated impedance of $50\ \Omega$ at 5.4 GHz with a length of 13.18 mm and a diameter of 0.511 mm (see Figure 15C and Figure 15D). It is also located half a wavelength away from the inside corner of the reflector [29]. The feed is switched between either a $50\ \Omega$ or short-circuit terminator using an RF switch [21]. The background of the electronically modulated reflector is lined with RF absorber foam, and the rest of the setup is identical to the one described in Section 4.2 with the Tx and Rx antennas placed closer to the reflector to compensate for its smaller size (see Figure 15A and 15B). The contrast in Rx power between the reflector states and the background clutter with no reflector can be seen in Figure 16B.

4.3.2 Results. In Figure 16A, the reflector passively modulates the reflected Tx signal at a bit rate of 200 bps, which is sufficient to transmit multiple bits over the course of a satellite pass. The amplitude difference between the ON and OFF states from the electronically modulated corner reflector

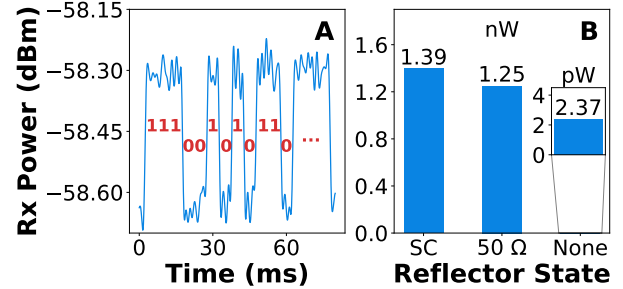


Figure 16: Electronic Modulation Result. (A) A 7-bit Barker code followed by a 5-bit payload is transmitted. (B) The signal is near zero when no reflector is present (None), and the reflector is more absorptive when connected to $50\ \Omega$ compared to short-circuit (SC).

is less pronounced than its mechanical counterpart (about 0.5 dB change), but this can likely be improved using a better-matched antenna since the Tx frequency transmitted in the experiment was 5.75 GHz instead of the 5.4 GHz the antenna was tuned to. The only power requirement of the device comes from the RF switch ($<3\ \mu\text{W}$ [21]), therefore it can function with orders of magnitude less energy than even the lowest-power IoT satellite solutions that use active Tx transmissions [43]. This makes modulating reflectivity with impedance matching a promising approach to achieving passive ground-to-satellite communication.

4.4 Processing Results

4.4.1 Implementation. Level 0 Sentinel-1 data was downloaded [35] and processed using backprojection algorithm code to convert the IQ samples into compressed single-look complex images [48]. The code was adapted for this work to implement subaperture processing. The resulting images are measures of the power of the backscattered signals, and the SCR of the target was analyzed using MATLAB [27]. Data provided in this paper uses the relative power numbers, as we are interested in the relative changes between images rather than their absolute values. They can be converted into units of watts after accounting for the antenna gain pattern, range, and number of data points used to generate the image.

4.4.2 Results. To evaluate the effectiveness of subaperture processing, we first look at the behavior of a static corner reflector with an increasing number of sublooks. In Figure 17, one of the sublook images of a $4' \times 4'$ reflector, as shown in Figure 12D deployed in a grassy field, is shown after processing with N sublooks where $N = 1, 2, 4, 8, 16, 32, 64$, and 128. In these images, the range and azimuth directions are not fully aligned with the pixel axes. The azimuth direction is tilted slightly in the clockwise direction from the vertical axis. As expected, the reflector has reduced resolution in the azimuth

direction, as seen by how the reflector is stretched, with larger values of N , and also has visibly reduced SCR.

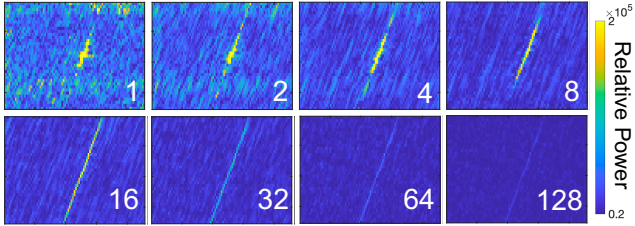


Figure 17: 4'x4' Corner Reflector in Sublook Images after being Processed into N Sublooks. Each image is annotated with the total number of sublooks that were processed from the aperture. More sublooks decreases the azimuth resolution of the image and the reflector's SCR.

For the points within these sub-images, each pixel uses an aperture with an original length of about 200 azimuth lines. Therefore, being able to discern the 4'x4' reflector from the image using so few samples per image shows that despite the short period of time available and limited samples, this technique is scalable. Using a 4'x4' reflector and 128 subapertures with a total aperture time of 100 ms, would equate to a data rate of 1280 bits per second. In Figure 18A, we evaluate quantitatively how the SCR reduces with the total number of azimuth sublooks used. Figure 18B analyzes the SCR of the reflector in each of the eight sublook images.

Figure 18A shows the SCR degrading as the number of sublooks is increased. Figure 10 shows that if the background clutter is constant, the SCR remains the same no matter how many looks are used. Since the clutter varies significantly in the field and the reflector was placed in a low-clutter environment originally, the background clutter increases relative to the reflector signal as the number of looks increases. Using the azimuth resolution equation from Section 3.4, the original azimuth resolution of the image when $N=1$ is 22 m, increases to 2816 m after sublooking 128 times. Therefore, much more clutter will be averaged into the background due to the coarser azimuth resolution. As such, there is a trade-off between the SCR and the amount of data that can be sent. Figure 18B shows that the SCR is maintained to within a dB (the accuracy of Sentinel-1) for each of the eight sublooks produced after splitting the aperture $N=8$ times [7], matching the derived theoretical analysis.

Next, we analyze the performance of a modulating reflector in the field. The mechanically modulating reflector was deployed in two scenarios, statically in its ON state and with the panels modulating between its ON and OFF states at a period of 100 ms. For this specific deployment site and relative orbit path, the reflector location was imaged for about 100 ms, meaning that there was time for a single ON/OFF

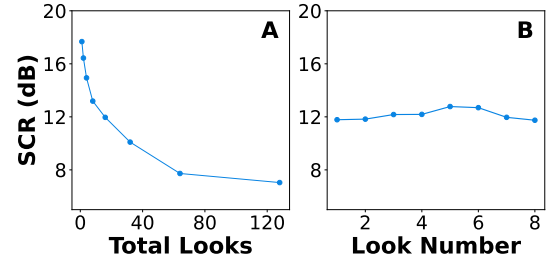


Figure 18: Subaperture SCR Analysis. Average SCR as 4'x4' corner reflector is evaluated (A) with respect to the total number of sublooks and (B) for each of the $N=8$ sublooks.

period. The static deployment in Figure 19A shows up quite brightly while in Figure 19B, the same reflector modulating has a greatly reduced RCS. These results demonstrate that by either setting the reflector to static or modulating states, the RCS can be used to detect changes in reflectivity (i.e. 0 and 1-bit transmissions).

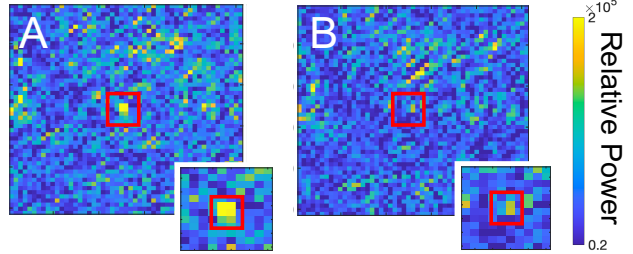


Figure 19: Static vs. Modulating Reflector The mechanically modulated reflector deployed (A) statically in its ON state and (B) switching with a 100 ms period.

In this experiment, we have successfully shown that the mechanically modulated reflector can be detected in the field during a Sentinel-1 pass, and we can control its reflected signal amplitude by changing the state of the reflector. This demonstrates ASK modulation in the field for a single bit of information. As shown in Figure 19B, the modulating reflector has a small SCR even while using the full aperture. As such, the reduction in SCR after subaperture processing makes it challenging to detect its modulation conclusively. This is primarily due to the increased clutter for that particular deployment location and rainy weather conditions. This may be addressed in future work by using a larger RCS target (i.e., a larger corner reflector) with a faster modulation speed to make it easier to evaluate the performance of subaperture processing on a modulating target.

5 RELATED WORK

This section describes the related technologies that have been individually investigated by prior work, which include IoT satellite connectivity, SAR background clutter processing, and modulated reflective surfaces:

- **IoT Satellite Connectivity.** The idea of connecting remote IoT devices to satellites has been well-explored by many commercial start-ups [43, 42, 32]. However, active radios that transmit enough power to communicate with satellites require watts of power, which is orders of magnitude more than what typical energy-harvesting and battery-constrained systems could afford [39]. Even state-of-the-art low-power satellite connectivity devices like Swarm M138 use upwards of 3.3 W during active transmission [43], and the cost of these devices can also be substantial due to the use of private satellite networks. This makes developing passive, low-cost communication methods with open-sourced satellites such as Sentinel-1 motivating for the IoT community.
- **Corner Reflector Deployment Algorithm.** Prior work [19] introduced a background clutter processor using SnapPy [18] to create SCR maps of areas to optimize corner reflector deployment. SARComm’s approach deviates from prior work by using the desired SCR as an input to allow the user to specify a requirement for the communication system.
- **Modulated Reflective Surfaces.** Other works that focused on military applications, such as [46], provided insights into how one might construct an active surface that selectively absorbs RF waves of specific frequencies to perform SAR jamming. They were able to achieve amplitude modulation of backscattered SAR signal using an active frequency selective surface (AFSS) constructed from bow-tie antennas and PIN diodes. However, their processing was tested in the lab with stationary radar units and simulated on existing measured data sets. Existing systems related to metamaterial surfaces for signal modulation are also only evaluated in simulation or in lab-scale settings [15, 12, 16, 14]. This makes deploying similar modulated surfaces for ground-to-satellite communication in the field an interesting area to explore.

6 FUTURE WORK

In this section, we discuss opportunities for future work to enable practical deployments of satellite backscatter communication systems:

- **Increasing Data Rate:** Deploying multiple reflectors can be used to boost the data rate over a single pass. While the reflectors should not be deployed closely in the azimuth direction, they can be very close to each other in the range direction since subaperture processing erodes only in the azimuth direction. In addition, phase information could be used to implement more complex modulation schemes beyond ASK. There is also another opportunity to double the number of communication channels available by effectively modulating both radar polarizations.

- **Reflector Improvement:** In order to improve the minimum RCS, state contrast, and switching speed of the system, new types of electronically modulated smart surfaces should be explored to create a larger RCS. This will further enable the more complex modulation schemes mentioned above by controlling the phase and polarizations of the SAR signals.
- **End-to-End System Demonstration:** Due to the challenges of conducting field experiments and adapting SAR processing for communication, this work’s focus has been the development of the components that make satellite backscatter communication possible. Future work will target integrating the deployment algorithm, modulated on-ground target, and data processing pipeline into an end-to-end system and demonstrate its functionalities.

7 CONCLUSION

This paper presents SARComm, the first wireless communication system to enable passive ground-to-satellite connectivity by leveraging existing spaceborne SAR systems. We demonstrate that corner reflectors can be effectively modulated to transmit information by changing their RCS, and these changes can be observed by the Sentinel-1 satellite as far as 693 km away. To improve performance, we construct a deployment algorithm that optimizes the corner reflector placement and develop a SAR data processing pipeline to extract information bits by splitting a single SAR image into multiple sublooks. SARComm lays the groundwork for enabling ultra-low power satellite connectivity in resource-constrained environments, which takes the first step to realizing the vision of ubiquitous global communication.

REFERENCES

- [1] 80/20. 2024. T-slotted profiles. <https://8020.net/framing-options/t-slotted-profiles.html>. (2024).
- [2] European Space Agency. 2023. About space debris. https://www.esa.int/Space_Safety/Space_Debris/About_space_debris. (2023).
- [3] European Space Agency. 2023. Dataproducts. <https://sentinels.copernicus.eu/web/sentinel/missions/sentinel-1/data-products>. (2023).
- [4] European Space Agency. 2024. Level-1 interferometric wide swath slc products. <https://sentinels.copernicus.eu/web/sentinel/technical-guides/sentinel-1-sar/products-algorithms/level-1/single-look-complex/interferometric-wide-swath>. (2024).
- [5] European Space Agency. 2023. Mission navigator. https://www.esa.int/ESA/Our_Missions. (2023).
- [6] European Space Agency. 2024. Orbit. <https://sentinels.copernicus.eu/web/sentinel/missions/sentinel-1/satellite-description/orbit>. (2024).
- [7] European Space Agency. 2024. Performance. <https://sentinel.esa.int/web/sentinel/technical-guides/sentinel-1-sar/sar-instrument/performance>. (2024).
- [8] European Space Agency. 2024. Sar instrument. <https://sentinels.copernicus.eu/web/sentinel/technical-guides/sentinel-1-sar/sar-instrument>. (2024).
- [9] The European Space Agency. 2024. Sentinel application platform. <https://earth.esa.int/eogateway/tools/snap>. (2024).

[10] WC Anderson. 1985. *The effect of varying the internal angle of a dihedral corner reflector*. Department of Defence, Defence Science and Technology Organisation ...

[11] Ansys. 2024. Ansys hfss. <https://www.ansys.com/products/electronics/ansys-hfss>. (2024).

[12] Venkat Arun and Hari Balakrishnan. 2020. {Rfocus}: beamforming using thousands of passive antennas. In *17th USENIX symposium on networked systems design and implementation (NSDI 20)*, 1047–1061.

[13] DARRELL L Ash. 1992. A comparison between ook/ask and fsk modulation techniques for radio links. *RF Monolithic Inc, Dallas, TX, USA, Tech. Rep.*

[14] Lili Chen, Wenjun Hu, Kyle Jamieson, Xiaojiang Chen, Dingyi Fang, and Jeremy Gummesson. 2021. Pushing the physical limits of {iot} devices with programmable metasurfaces. In *18th USENIX Symposium on Networked Systems Design and Implementation (NSDI 21)*, 425–438.

[15] Kun Woo Cho, Yasaman Ghasempour, and Kyle Jamieson. 2022. Towards dual-band reconfigurable metasurfaces for satellite networking. In *Proceedings of the 21st ACM Workshop on Hot Topics in Networks*, 17–23.

[16] Kun Woo Cho, Mohammad H Mazaheri, Jeremy Gummesson, Omid Abari, and Kyle Jamieson. 2021. Mmwall: a reconfigurable metamaterial surface for mmwave networks. In *Proceedings of the 22nd International Workshop on Mobile Computing Systems and Applications*, 119–125.

[17] The Physics Classroom. 2023. Mathematics of satellite motion. <https://www.physicsclassroom.com/class/circles/Lesson-4/Mathematics-of-Satellite-Motion>. (2023).

[18] Marc Culler, Nathan M. Dunfield, Matthias Goerner, and Jeffrey R. Weeks. 2023. SnapPy, a computer program for studying the geometry and topology of 3-manifolds. Available at <http://snappy.computop.org> (DD/MM/YYYY). (2023).

[19] Richard Czirkhardt, Hans Van Der Marel, and Juraj Papco. 2021. GECORIS: an open-source toolbox for analyzing time series of corner reflectors in InSAR geodesy. *Remote Sensing*, 13, 5, (Mar. 2, 2021), 926. doi: 10.3390/rs13050926.

[20] Analog Devices. 2016. Adg918/adg919. https://www.mouser.com/datasheet/2/609/ADG918_919-3120314.pdf. (2016).

[21] Analog Devices. 2024. Adg919. <https://www.analog.com/en/products/adg919.html>. (2024).

[22] Armin Walter Doerry. 2014. Reflectors for SAR performance testing. Tech. rep. Sandia National Lab.(SNL-NM), Albuquerque, NM (United States).

[23] Giorgio Franceschetti and Riccardo Lanari. 2018. *Synthetic Aperture Radar Processing*. CRC Press.

[24] Christoph Gisinger, Adrian Schubert, Helko Breit, Matthew Garthwaite, Ulrich Balss, Martin Willberg, David Small, Michael Eineder, and Nuno Miranda. 2021. In-depth verification of sentinel-1 and terrasar-x geolocation accuracy using the australian corner reflector array. *IEEE Transactions on Geoscience and Remote Sensing*, 59, 2, 1154–1181. doi: 10.1109/TGRS.2019.2961248.

[25] gobILDA. 2024. 2000 series dual mode servo (25-4, super speed). <https://www.gobilda.com/2000-series-dual-mode-servo-25-4-super-speed/>. (2024).

[26] Pasternack Enterprises Inc. 2019. 4.9-5.8 GHz dual polarized 30dBi dish antenna datasheet. <https://www.pasternack.com/images/ProductPDF/PE51PD1002.pdf>. (2019).

[27] [SW] The MathWorks Inc., MATLAB version: 9.10.0 (R2021a) 2024. URL: <https://www.mathworks.com>.

[28] Matthias Jauvin, Yajing Yan, Emmanuel Trouvé, Bénédicte Fruneau, Michel Gay, and Blaise Girard. 2019. Integration of corner reflectors for the monitoring of mountain glacier areas with sentinel-1 time series. *Remote Sensing*, 11, 8, 988.

[29] John D Kraus. 1940. The corner-reflector antenna. *Proceedings of the IRE*, 28, 11, 513–519.

[30] [SW] Google Maps, Satellite Image of Grassy Field 2024. URL: <https://www.google.com/maps>.

[31] United Nations. 2021. Itu: 2.9 billion people still offline. <https://www.un.org/en/delegate/itu-29-billion-people-still-offline>. (2021).

[32] Hubble Network. 2023. Hubble network. <https://hubblenetwork.com/>. (2023).

[33] National Radio Astronomy Observatory. 2023. Radio frequency interference. <https://public.nrao.edu/telescopes/radio-frequency-interference/>. (2023).

[34] Avionics Department of the Naval Warfare Center Weapons Division. 2013. Electronics warfare and radar systems engineering handbook. <https://apps.dtic.mil/sti/tr/pdf/ADA617071.pdf>. (2013).

[35] The University of Alaska Fairbanks. 2024. Alaska satellite facility. <https://asf.alaska.edu/>. (2024).

[36] Sentinel Online. 2024. Level-1. <https://sentinels.copernicus.eu/web/sentinel/user-guides/sentinel-1-sar/product-types-processing-levels/level-1>. (2024).

[37] Tarig Ibrahim Osman and Abdelrasoul Jabar Alzubaidi. 2014. Analysis of radar cross sectional area of corner reflectors.

[38] K. Ouchi. 1985. On the multilook images of moving targets by synthetic aperture radars. *IEEE Transactions on Antennas and Propagation*, 33, 8, 823–827. doi: 10.1109/TAP.1985.1143684.

[39] Joseph A Paradiso and Thad Starner. 2005. Energy scavenging for mobile and wireless electronics. *IEEE Pervasive computing*, 4, 1, 18–27.

[40] Leonard J. Porcello, Norman G. Massey, Richard B. Innes, and James M. Marks. 1976. Speckle reduction in synthetic-aperture radars. *J. Opt. Soc. Am.*, 66, 11, (Nov. 1976), 1305–1311. Publisher: Optica Publishing Group. doi: 10.1364/JOSA.66.001305.

[41] [SW] Microsoft Open Source, Matt McFarland, Rob Emanuele, Dan Morris, and Tom Augspurger, microsoft/PlanetaryComputer: October 2022 version 2022.10.28, Oct. 2022. doi: 10.5281/zenodo.7261897, URL: <https://doi.org/10.5281/zenodo.7261897>.

[42] Starlink. 2023. Technology. <https://www.starlink.com/technology>. (2023).

[43] SWARM. 2023. Swarm modem product manual. <https://swarm.space/wp-content/uploads/2022/09/Swarm-M138-Modem-Product-Manual.pdf>. (2023).

[44] The European Space Agency. 2023. Introducing sentinel-1. https://www.esa.int/Applications/Observing_the_Earth/Copernicus/Sentinel-1/Introducing_Sentinel-1. (2023).

[45] ASF Vertex. 2023. What is sar. <https://asf.alaska.edu/information/sar-information/what-is-sar/>. (2023).

[46] Junjie Wang, Dejun Feng, Letao Xu, Ran Zhang, and Weidong Hu. 2019. Synthetic aperture radar target feature modulation using active frequency selective surface. *IEEE Sensors Journal*, 19, 6, 2113–2125. doi: 10.1109/JSEN.2018.2886013.

[47] Xiaoying Yang, Jacob Sayono, and Yang Zhang. 2023. Cubesense++: smart environment sensing with interaction-powered corner reflector mechanisms. In *Proceedings of the 36th Annual ACM Symposium on User Interface Software and Technology (UIST '23) Article 78*. Association for Computing Machinery, San Francisco, CA, USA, 12 pages. ISBN: 9798400701320. doi: 10.1145/3586183.3606744.

[48] Howard A. Zebker. 2017. User-friendly insar data products: fast and simple timeseries processing. *IEEE Geoscience and Remote Sensing Letters*, 14, 11, 2122–2126. doi: 10.1109/LGRS.2017.2753580.